Journal of Physics: Conference Series **455** (2013) 012013 doi:10.1088/1742-6596/455/1/012013

Search for the SM Higgs boson in the diboson decay modes with the ATLAS detector

German Carrillo-Montoya, on behalf of the ATLAS Collaboration
University of the Witwatersrand. Conference proceedings, International Workshop on Discovery Physics at the LHC 2012, Kruger South Africa

E-mail: montoya@cern.ch

Abstract. A Higgs boson search in the $H \to \gamma\gamma$, $H \to ZZ^{(*)} \to 4\ell$ and $H \to WW^{(*)} \to \ell\nu\ell\nu$ decay modes has been performed using proton-proton collisions collected in 2011 and 2012 with the ATLAS detector. Updated results on the observed resonance using up to 4.7 fb^{-1} of $\sqrt{s} = 7$ TeV and 13.0 fb^{-1} of $\sqrt{s} = 8$ TeV data including first measurement of its properties are presented and discussed.

1. Introduction

The Standard Model (SM) of particle physics [1–4] has been extensively probed by many experiments in the last decades. In the SM, the Brout-Englert-Higgs mechanism is the source of electroweak symmetry breaking and results in the appearance of the Higgs boson [5–7]. This note describes the updated results of the search of the Higgs boson in the diboson decay modes with the ATLAS detector. Section 2 provides a short description of the production mechanism that create the Higgs boson in proton-proton colliders. Sec. 3 give a short description of the ATLAS detector. The results of the $H \to \gamma\gamma$ channel [8, 9] using 4.8 fb^{-1} of $\sqrt{s}$ =7 TeV and 5.9 fb^{-1} of $\sqrt{s}$ =8 TeV data are described in Sec. 4, while the results obtained in the $H \to ZZ^{(*)} \to 4\ell$ search [8, 10] using an integrated luminosity of 4.8 fb^{-1} of $\sqrt{s}$ =7 TeV and 5.8 fb^{-1} of $\sqrt{s}$ =8 TeV are shown in Sec. 5. Finally the updated measurements of the $H \to WW^{(*)} \to \ell\nu\ell\nu$ analysis [11,12] where 13.0 fb^{-1} of $\sqrt{s}$ =8 TeV data was used are given in Sec. 6.

2. Higgs boson production at the LHC

In $p-p$ collisions the Higgs boson can be created through different production mechanisms. The fusion of gluons through a quark loop is the dominant process given the high gluon luminosities, then the vector bosons fusion (VBF) emitted from incoming quarks with a distinct signature of two high transverse momentum (p_{T}) jets, the so called associated production or Higgs-strahlung where a W or a Z boson is present in the final state. Finally, with a much smaller cross section, the Higgs boson can also be produced accompanied by a top quark pair. In Fig. 1 Feynman diagrams are shown for the three most important processes. The production cross sections and decay branching fractions vary as function of the Higgs boson mass hypothesis (m_{H}). In Tab. 1 the production cross section for the gluon-gluon-fusion (ggF) and VBF are shown for $p-p$ collisions at $\sqrt{s}$ =7 and $\sqrt{s}$ =8 TeV. The state for the art high order electroweak, QCD, gluon re-summation, interference and other corrections are taken from [13]. The large instantaneous

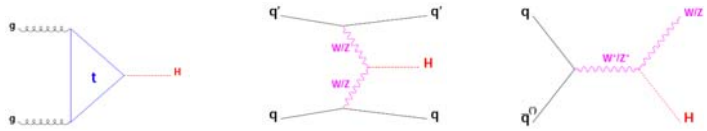

Figure 1. Feynman diagrams for the leading order Higgs boson production mechanisms at the LHC. Left: Gluon-gluon fusion trough and top quark loop. Centre: Vector boson fusion. Right: Associated production with a vector boson (W/Z).

luminosities at the LHC imply a large number of soft collisions per bunch crossing in addition to the hard scattering (event pile-up), this effects are included in the simulations used in the different analyses, a more comprehensive set of details of the simulation chain can be found in [8].

Table 1. Higgs boson production cross sections at the LHC for the ggF and VBF production mechanism at $\sqrt{s}$ =7 and $\sqrt{s}$ =8 TeV centre of mass energies [13].

$\sqrt{s}$ [TeV]	σ_{ggF} [pb]	σ_{VBF} [pb]	$\sigma_{pp\to H}$ [pb]
7	15.3	1.2	17.5
8	19.5	1.6	22.3

3. The ATLAS detector

The ATLAS detector [14] is a multi-purpose particle physics detector with forward-backward symmetric cylindrical geometry[1]. The inner tracking detector (ID) covers $|\eta| < 2.5$ and consists of a silicon pixel detector, a silicon micro-strip detector, and a transition radiation tracker (TRT). The ID is surrounded by a thin superconducting solenoid providing a 2 T axial magnetic field. A high-granularity lead/liquid-argon (LAr) sampling calorimeter measures the energy and the position of electromagnetic showers within $|\eta| < 3.2$. LAr sampling calorimeters are also used to measure hadronic showers in the end-cap ($1.5 < |\eta| < 3.2$) and forward ($3.1 < |\eta| < 4.9$) regions, while an iron/scintillator tile calorimeter measures hadronic showers in the central region ($|\eta| < 1.7$). The muon spectrometer (MS) surrounds the calorimeters and consists of three large superconducting air-core toroid magnets, each with eight coils, a system of precision tracking chambers ($|\eta| < 2.7$), and fast trigger chambers. A three-level trigger system selects events to be recorded for offline analysis.

4. $H \to \gamma\gamma$

The search of the Higgs boson in the diphoton final state is perform in the mass range between 110 and 150 GeV. The smoothly falling background in the invariant $m_{\gamma\gamma}$ is mainly made of SM $\gamma\gamma$, production, with subleading contributions from $\gamma + jets$, $jet - jet$ and Drell-Yan processes, where jets (or e) are misidentified as photons.

4.1. Selection

Photons are reconstructed from electromagnetic clusters using a neural-net algorithm in the 2011 data, and a cut based optimised to minimised the impact of pile-up in 2012. The photon candidates are required to have transverse energy E_{T} >40 and 30 GeV and to be in the fiducial

[1] The ATLAS experiment uses a right-handed coordinate system with its origin at the nominal interaction point. The z-axis is along the beam pipe, the x-axis points to the centre of the LHC ring and the y-axis is defined as pointing upwards. Polar coordinates (r,ϕ) are used in the transverse plane, ϕ being the azimuthal angle around the beam pipe. The pseudo-rapidity η is defined as $\eta = -\ln[\tan(\theta/2)]$ where θ is the polar angle.

volume. Details of the photon reconstruction and the object selection are given in [9]. To enhanced the sensitivity, ten mutually exclusive categories are created based on mass resolution, or the presence of two jets compatible with the VBF production topology. Table 2 list various categories as well as the number of expected signal events in the $\sqrt{s}$ =7 and $\sqrt{s}$ =8 TeV data sets.

Table 2. Number of events in the data (N_D) and expected number of signal events (N_S) for $m_{\rm H}$=126.5 GeV from the $H \to \gamma\gamma$ analysis, for each category in the mass range 100-160 GeV. The mass resolution FWHM is also given for the $\sqrt{s}$ =8 TeV data. The Higgs boson production cross section multiplied by the branching ratio into two photons ($\sigma \times BR(H \to \gamma\gamma)$) is listed for $m_{\rm H}$=126.5 GeV. The statistical uncertainties on N_S and FWHM are less than 1% [8].

$\sqrt{s}$	7 TeV		8 TeV		
$\sigma \times B(H \to \gamma\gamma)$ [fb]		39		50	FWHM
Category	$N_{\rm D}$	$N_{\rm S}$	$N_{\rm D}$	$N_{\rm S}$	[GeV]
Unconv. central, low $p_{{\rm T}t}$	2054	10.5	2945	14.2	3.4
Unconv. central, high $p_{{\rm T}t}$	97	1.5	173	2.5	3.2
Unconv. rest, low $p_{{\rm T}t}$	7129	21.6	12136	30.9	3.7
Unconv. rest, high $p_{{\rm T}t}$	444	2.8	785	5.2	3.6
Conv. central, low $p_{{\rm T}t}$	1493	6.7	2015	8.9	3.9
Conv. central, high $p_{{\rm T}t}$	77	1.0	113	1.6	3.5
Conv. rest, low $p_{{\rm T}t}$	8313	21.1	11099	26.9	4.5
Conv. rest, high $p_{{\rm T}t}$	501	2.7	706	4.5	3.9
Conv. transition	3591	9.5	5140	12.8	6.1
2-jet	89	2.2	139	3.0	3.7
All categories (inclusive)	23788	79.6	35251	110.5	3.9

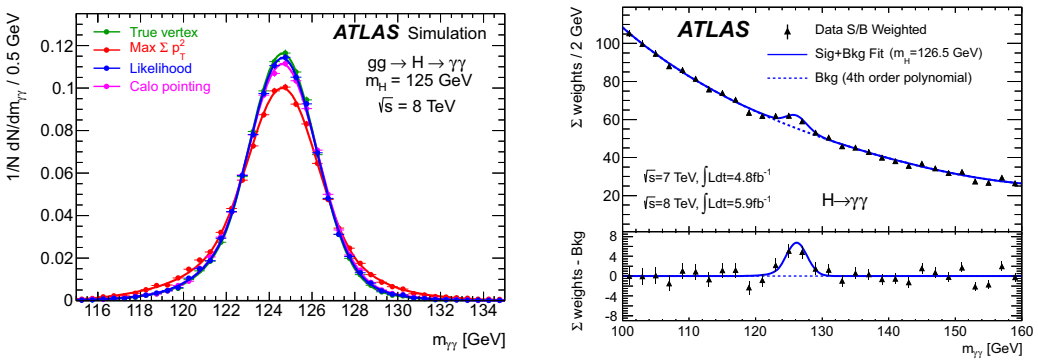

Figure 2. Left: Distribution of the expected diphoton mass for $H \to \gamma\gamma$ signal events as a function of the algorithm used to determine the longitudinal vertex position of the hard-scattering event. The use of the calorimeter information, labelled as "Calo pointing" is fully adequate to reach the optimal achievable mass resolution labelled as "True vertex". The likelihood described in [8], combining this information with the primary vertex information from the tracking, provides similar mass resolution. Right: The weighted distribution of invariant mass of diphoton candidates for the combined $\sqrt{s} = 7$ TeV and $\sqrt{s} = 8$ TeV data samples. The weight w_i for category i from [1, 10] is defined to be $\ln(1+S_i/B_i)$, where S_i is 90% of the expected signal for $m_{\rm H} = 126.5$ GeV, and B_i is the integral, in a window containing S_i, of a background-only fit to the data. The values S_i/B_i have only a mild dependence on $m_{\rm H}$. The result of a fit to the data of the sum of a signal component fixed to $m_{\rm H}$=126.5 GeV and a background component described by a fourth-order Bernstein polynomial is superimposed. The bottom inset displays the residuals of the data with respect to the fitted background component [8].

4.2. Results

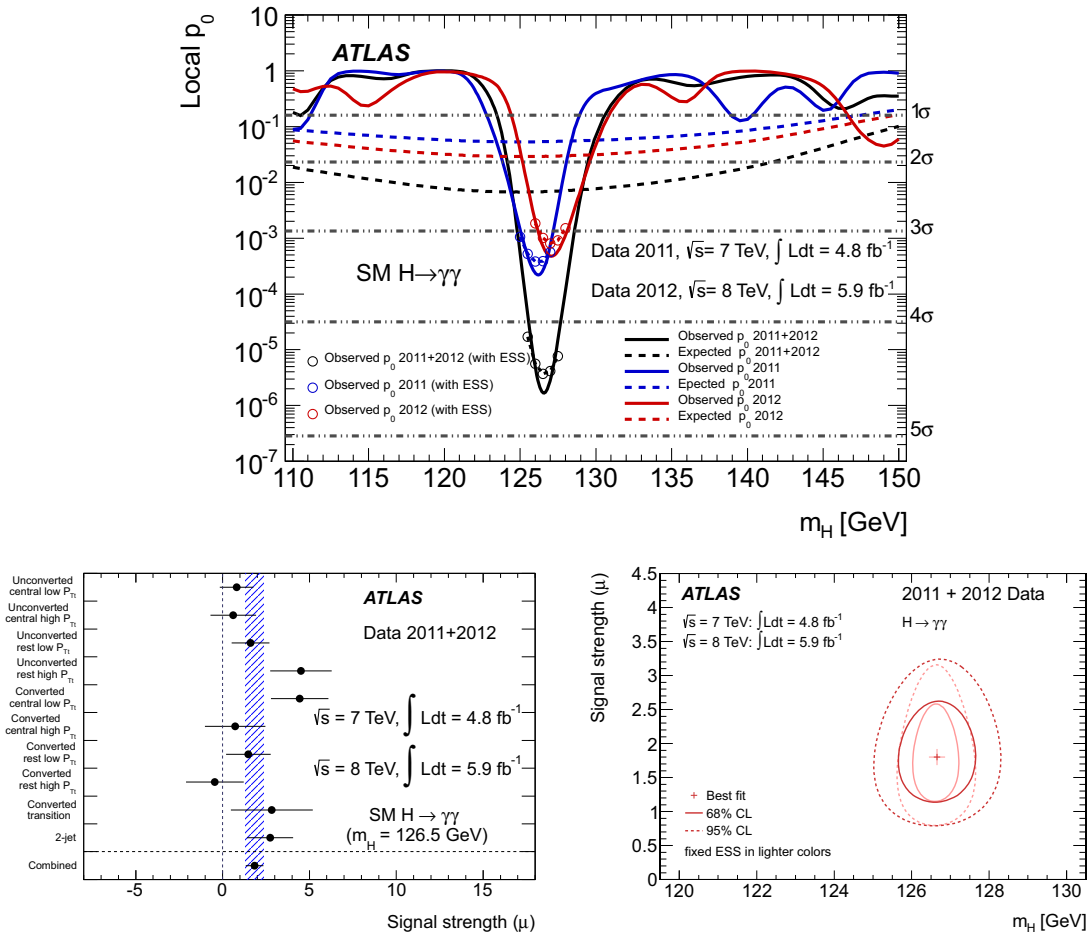

Figure 3. Top: Expected and observed local p_0 values for a SM Higgs boson as a function of the hypothesised Higgs boson mass for the combined analysis and for the $\sqrt{s} = 7$ TeV and $\sqrt{s} = 8$ TeV data samples separately. The observed p_0 including the effect of the photon energy scale uncertainty on the mass position is included via pseudo-experiments and shown as open circles. Bottom left: Best fit value for the signal strength in the different categories at $m_{\rm H}$= 126.5GeV for the combined $\sqrt{s} = 7$ TeV and $\sqrt{s} = 8$ TeV data samples. The blue band corresponds to the error of the combined result. Bottom right: Confidence intervals contours in the $(\mu, m_{\rm H})$ plane. The 68% and 95% CL contours are for the combined $\sqrt{s} = 7$ TeV and $\sqrt{s} = 8$ TeV analysis. The light lines indicate the effect of holding constant at their best-fit values the nuisance parameters which describe the energy scale systematic (ESS) uncertainties in the likelihood function [8].

The $\sqrt{s} = 7$ and $\sqrt{s}$ =8 TeV combined distribution of the invariant mass, $m_{\gamma\gamma}$, is shown in Fig. 2 (Left). The presence of the excess is statistically quantified by performing an unbinned likelihood fit as described in [9]. Figure 3 (Top) shows the local p_0 value including the possible effect of energy scale systematics. The $\sqrt{s}$ =7 TeV p_0 corresponds to 3.5σ, while the $\sqrt{s}$ =8 TeV p_0 corresponds to a 3.4σ and their combination to 4.5σ. The best fitted mass is 126.5 GeV and its signal strength, $\hat{\mu}$ =1.8$\pm$0.5. Figure 3 (Bottom left) gives the strength fitted values for the various categories. The effect of the energy scale systematic on the measured mass can be seen in Fig. 3 (Bottom right). Compatible with the SM Higgs boson prediction within 2σ.

5. $H \to ZZ^{(*)} \to 4\ell$

The $H \to ZZ^{(*)} \to 4\ell$ analysis explores a mass range between 110 and 600 GeV. The good lepton momentum resolution and the clean signature of four charged leptons ($\ell = e, \mu$) coming from the Z bosons decay allows a powerful signal to background separation. The dominant background source is the SM production of $ZZ^{(*)}$, which is an irreducible background. The production of a Z together with a pair of light or heavy jets is the second most important background. A small contribution from top quark pair production is also expected.

5.1. Selection

Leptons are required to be within the fiducial volume and to have a transverse momentum, p_{T}, of at least 20,15,10 GeV for the three leading leptons, and at least 7(6) GeV for the final muon(electron). The lepton quadruplet must satisfy certain criteria that ensures they come from a $ZZ^{(*)}$ pair. Details of the required selections are given in [10]. Lepton isolation and impact parameter requirements are also imposed to reject both misidentified and leptons coming from semileptonic heavy flavour decays. Reducible backgrounds are measured using enriched control samples by relaxing/reversing quality requirements on the subleading lepton pairs, and the irreducible process is constraint during the fit by using the complete invariant $m_{4\ell}$ spectra including the so called single resonant $Z \to 4\ell$ process.

In Fig. 4 (Left) it is shown the invariant mass of the four lepton system for the combined data set. Table 3 shows the expected and observed number of events for the signal and different background components in a window of 5 GeV around $m_{4\ell}$ =125 GeV. The distribution of the candidates in the m_{12} (formed by the lepton pair closest to the on-shell Z boson mass), and m_{34} (invariant mass of the second lepton pair) plane is shown in Fig. 4 (Right).

5.2. Results

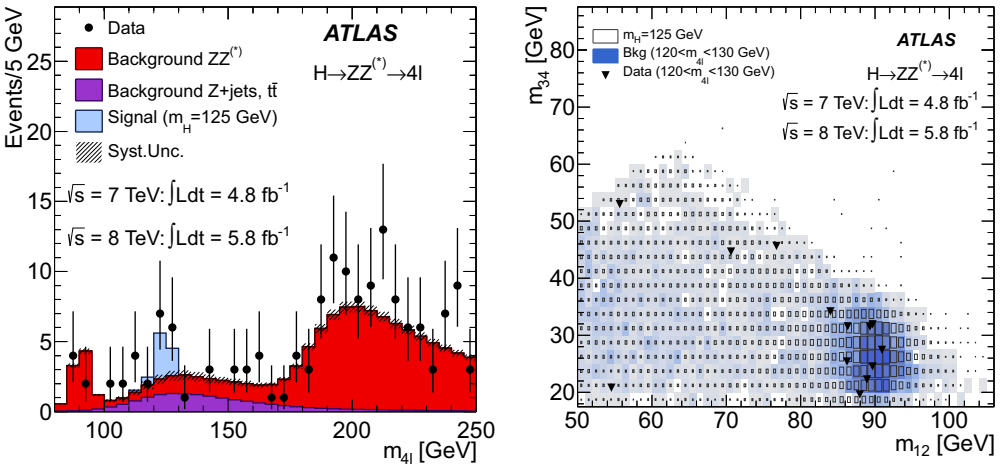

Figure 4. Left: The distribution of the four-lepton invariant mass, $m_{4\ell}$, for the selected candidates, compared to the background expectation in the 80 to 250 GeV mass range, for the combination of the $\sqrt{s} = 7$ TeV and $\sqrt{s} = 8$ TeV data. The signal expectation for a SM Higgs with m_{H}=125 GeV is also shown. Right: Distribution of the m_{34} versus the m_{12} invariant mass, before the application of the Z-mass constrained kinematic fit, for the selected candidates in the $m_{4\ell}$ range 120 to 130 GeV. The expected distributions for a SM Higgs with m_{H}=125 GeV (the sizes of the boxes indicate the relative density) and for the total background (the intensity of the shading indicates the relative density) are also shown [8].

Sensitivity is increased by splitting the analysis into four different lepton flavour combinations $(m_{12}; m_{34})$: $4\mu, 2\mu 2e, 2e2\mu$, and $4e$ where s/b and background compositions are different. The local p_0-values for the independent datasets and their combination as function of $m_{\rm H}$ are shown in Fig. 5 (Left). The likelihood fit of the combined $\sqrt{s} = 7$ TeV and $\sqrt{s} = 8$ TeV data indicates an excess of 3.6σ. In Fig. 5 (Right) the likelihood ratio contour plot in the $\hat{\mu}, m_{\rm H}$ is shown, the best fitted signal strength corresponds to 1.2±0.6, fully compatible with the SM within 1σ.

Table 3. The numbers of expected signal ($m_{\rm H}$=125 GeV) and background events, together with the numbers of observed events in the data, in a window of size ±5 GeV around 125 GeV, for the combined $\sqrt{s} = 7$ TeV and $\sqrt{s} = 8$ TeV data. [8].

	Signal	$ZZ^{(*)}$	$Z+$jets, $t\bar{t}$	Observed
4μ	2.09±0.30	1.12±0.05	0.13±0.04	6
$2e2\mu/2\mu2e$	2.29± 0.33	0.80±0.05	1.27±0.19	5
$4e$	0.90±0.14	0.44±0.04	1.09±0.20	2

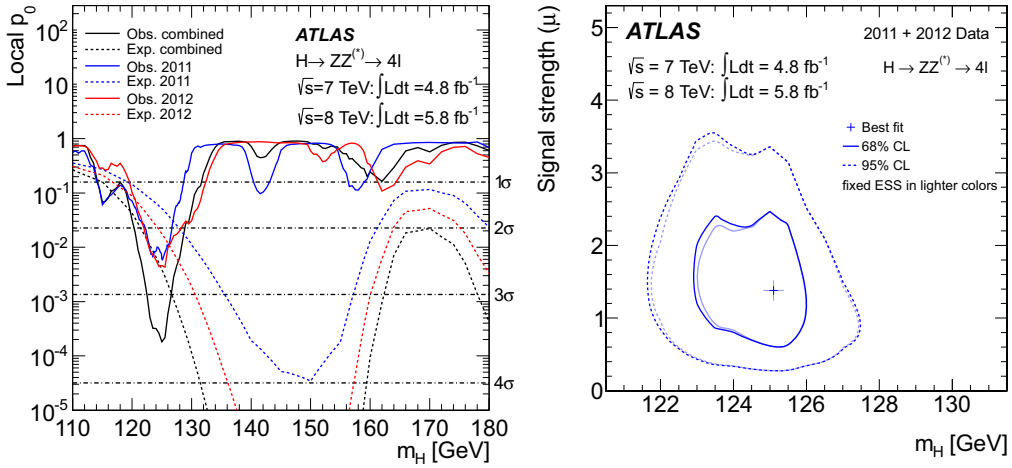

Figure 5. Left: The observed local p_0 for the combination of the 2011 and 2012 data sets (solid black line); the $\sqrt{s} = 7$ TeV and $\sqrt{s} = 8$ TeV data results are shown in solid lines (blue and red, respectively). The dashed curves show the expected median local p_0 for the signal hypothesis when tested at the corresponding $m_{\rm H}$. The horizontal dashed lines indicate the p_0 values corresponding to local significances of 1σ, 2σ, 3σ and 4σ. Right: Best fit values for μ and $m_{\rm H}$, and likelihood ratio contours that, in the asymptotic limit, correspond to 68% and 95% level contours in the $(\mu, m_{\rm H})$ plane. The light lines indicate the effect of holding constant at their best-fit values the nuisance parameters which describe the energy scale systematic uncertainties in the likelihood function [8].

6. $H \to WW^{(*)} \to \ell\nu\ell\nu$

The $H \to WW^{(*)} \to \ell\nu\ell\nu$ is the most sensitive analysis in the intermediate mass region (130-180 GeV). To properly normalise the complex background composition in the two lepton plus missing transverse energy ($E_{\rm T}^{miss}$) final state the analysis is divided according to the possible different flavour combinations and exclusive jet multiplicities. The results shown here correspond to an update of [11], where the opposite flavour final states in the 0- and 1-jet categories are revisited using 13 fb^{-1} of $\sqrt{s}$ =8 TeV data.

6.1. Selection

In the zero jet category, the dominant background process is the SM production of $WW^{(*)}$, it is followed by the top quark backgrounds and Drell-Yan process. Subleading contributions of $W + jets$, WZ and $W\gamma$ are also considered. The one jet category has similar processes, but the top quark backgrounds become more important, and some compositions also change like the larger relative presence of $Z \to \tau\tau$. The jet multiplicity and E_{T}^{miss} relative to the objects in the event are shown in Fig. 6.

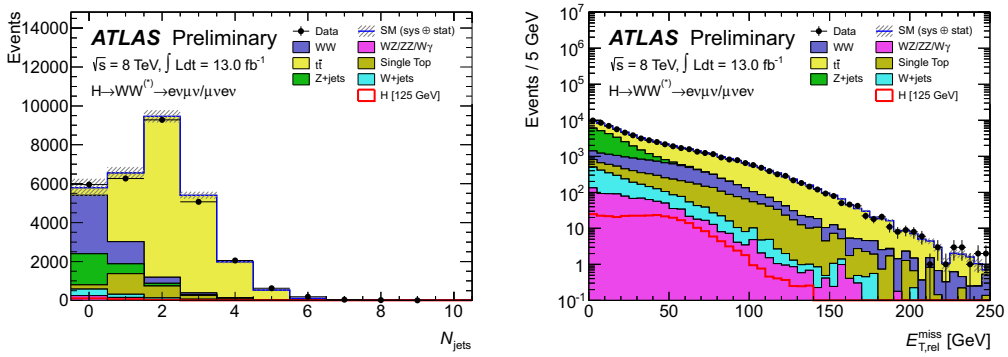

Figure 6. $E_{\mathrm{T}}^{\mathrm{miss,rel}}$ (Left) and multiplicity of jets (Right) for events satisfying the pre-selection criteria described in [12]. No $E_{\mathrm{T}}^{\mathrm{miss,rel}}$ requirement is applied in the $E_{\mathrm{T}}^{\mathrm{miss,rel}}$ distribution. Jets are required to fulfil $p_{\mathrm{T}} > 25$ GeV for $|\eta| < 2.5$ and $p_{\mathrm{T}} > 30$ GeV for $2.5 < |\eta| < 4.5$. The lepton channels are combined. The hashed area indicates the total uncertainty on the background prediction. The WW and top backgrounds are scaled to use the normalisation derived from the corresponding control regions described in the text. The expected signal for a SM Higgs boson with m_{H}=125GeV is superimposed [12].

A series of tight electron a muon identification criteria keeping leptons down to 25 GeV (15 GeV) in p_T for the leading (subleading) objects are applied. The event selection selects candidates compatible with two oppositely charged leptons each coming form a leptonic W decay, where the W and produced from a scalar object. Details about the object and event selection can be found in [12].

All the main backgrounds are normalised using control regions. The control regions are defined by selections similar to those used for the signal region but with some criteria reversed or modified to obtain signal-depleted samples enriched in a particular background. Some control regions have significant contributions from backgrounds other than the targeted one, which introduces dependencies among the background estimates. These correlations are taken into account in the WW control region where the top and $W + jets$ backgrounds are subtracted using their respective measurements. See [11] and [12] for full details on the background control samples and estimates.

6.2. Results

The presence of two neutrinos forbids the reconstruction of the Higgs boson invariant mass, therefore a transverse mass, m_{T}, is used as final discriminant variable. Figure 7 shows the m_{T} for the four different categories. The expected and observed number of events in the signal region for the zero and one jet categories are displayed in Tab. 4 As is was done for the channels previously presented, a statistical procedure is performed to quantify the size of the observed excess. Due to the poor resolution, driven by its final state, the $H \to WW^{(*)} \to \ell\nu\ell\nu$ channel has very little sensitivity to the Higgs mass hypothesis, other than the actual total signal yield.

Table 4. The observed numbers of events compared to the expectation from signal ($m_{\rm H}$125 GeV) and background after the full event selection, including a cut on the transverse mass of $0.75m_{\rm H} < m_{\rm T} < m_{\rm H}$. Data-derived normalisations of the backgrounds are included wherever applicable, as described in [12]. The uncertainties shown include both the statistical and systematic contributions, although the uncertainties on the control-region-derived backgrounds (WW, top in the H+1-jet analysis) do not include the uncertainty from the subtraction of other processes to the control region. The total uncertainty on the predicted background is calculated accounting for the correlations among the predictions, so the total does not correspond exactly to the sum in quadrature of the individual contributions. All numbers are summed over lepton flavours. [12].

	Signal	WW	$WZ/ZZ/W\gamma$	$t\bar{t}$	Single top	Drell-Yan	W+jets	Tot Bkg	Obs.
$H+0$ jet	45±9	242±32	26±4	16±2	11±2	4±3	34±17	334±28	423
$H+1$ jet	18±6	40±22	10±2	37±13	13±7	2±1	11±6	114±18	141

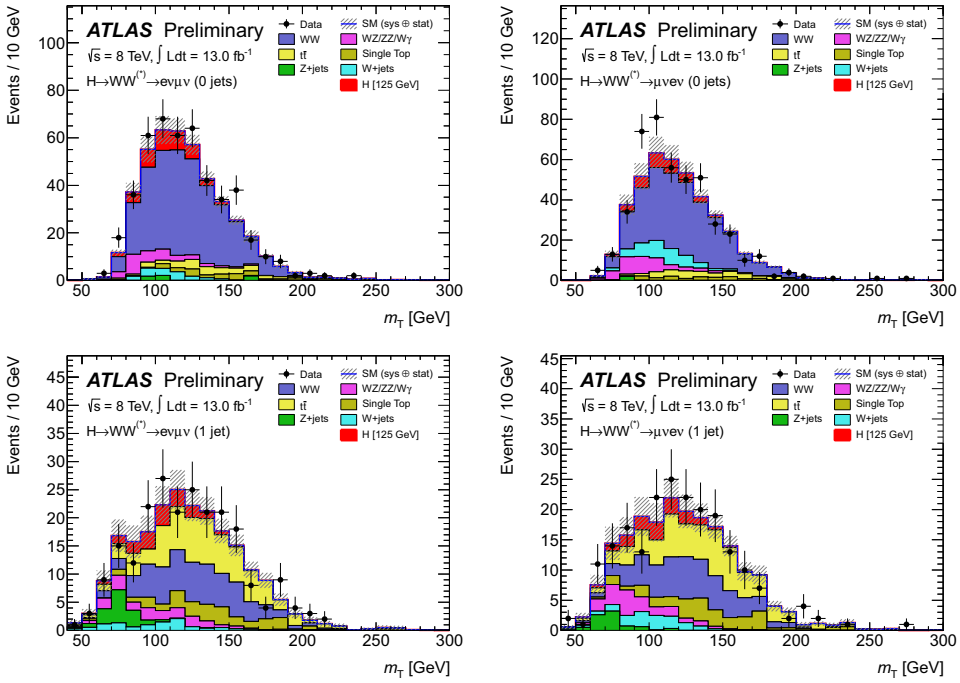

Figure 7. Transverse mass distribution in the zero jet (Top) and one jet (Bottom) channels, for events satisfying all criteria. The plots on the left show the events with a leading electron and the plots on the right show the events with a leading muon. The expected signal for a SM Higgs boson with $m_{\rm H}$ =125 GeV is added on top of the estimated total background. The W+jets background is estimated from data and WW, top and $Z \to \tau\tau$ backgrounds are scaled to use the normalisation derived from the corresponding control regions as described in the text. The hashed area indicates the total uncertainty on the total prediction [12].

In Fig. 8 (Left), the local p_0 is shown. At 125 GeV, an excess of 2.6σ is observed, with a signal strength $\hat{\mu}$ =1.5±0.6. The profiled likelihood contours of $m_{\rm H}$ and $\hat{\mu}$ for the three channels are shown in Fig. 8 (Right). All measured quantities are compatible among each other, as well as with a SM Higgs boson within 2σ.

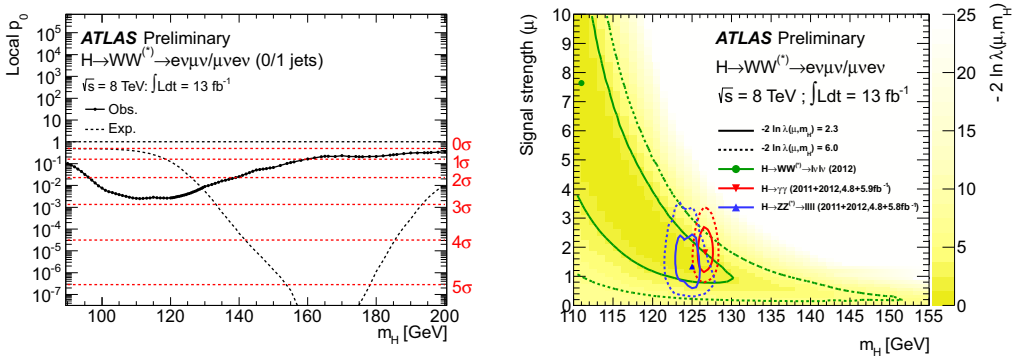

Figure 8. Left: observed (solid line) probability for the background-only scenario as a function of m_{H}. The dashed line shows the corresponding expectation for the signal+background hypothesis at the given value of m_{H}. Right: Approximate 68% and 95% two-dimensional likelihood ($\lambda(\mu, m_{\mathrm{H}})$) contours in the (μ, m_{H}) plane for the $H \to WW^{(*)} \to e\nu\mu\nu/\mu\nu e\nu$ zero jet and one jet data results with an integrated luminosity of 13 fb^{-1} at $\sqrt{s}$ =8 TeV. The results obtained for the $H \to ZZ^{(*)} \to 4\ell$ and $H \to \gamma\gamma$ analyses are overlaid, The yellow shading shows the $-\ln\lambda(\mu, m_{\mathrm{H}})$ values for $H \to WW^{(*)} \to e\nu\mu\nu/\mu\nu e\nu$ [12].

6.3. Summary

The updated results in the search for the SM Higgs boson in the $H \to \gamma\gamma$, $H \to ZZ^{(*)} \to 4\ell$ and $H \to WW^{(*)} \to \ell\nu\ell\nu$ decay modes with the ATLAS detector are presented. An excess compatible with the production of this particle is observed in the three cases, with local significances corresponding to 4.5σ in the diphoton final state, 3.6σ in the four lepton case, and 2.6σ in the $WW^{(*)}$ mode.

References

[1] S. L. Glashow, *Partial symmetries of weak interactions*, Nucl. Phys. **B 22** (1961) 579.
[2] S. Weinberg, *A model of leptons*, Phys. Rev. Lett. **19** (1967) 1264.
[3] A. Salam, *Elementary particle theory.* Almqvist and Wiksells, Stockholm, 1968.
[4] G. 't Hooft and M. Veltman, *Regularization and Renormalization of Gauge Fields*, Nucl. Phys. **B44** (1972) 189.
[5] F. Englert and R. Brout, *Broken symmetry and the mass of gauge vector mesons*, Phys. Rev. Lett. **13** (1964) 321–323.
[6] P. W. Higgs, *Broken symmetries and the masses of gauge bosons*, Phys. Rev. Lett. **13** (1964) 508–509.
[7] G. S. Guralnik, C. R. Hagen, and T. W. B. Kibble, *Global conservation laws and massless particles*, Phys. Rev. Lett. **13** (1964) 585–587.
[8] ATLAS Collaboration, *Observation of a new particle in the search for the standard model Higgs boson with the ATLAS detector at the LHC*, Phys. Lett. **B716** (2012) 1–29, `arXiv:1207.7214 [hep-ex]`.
[9] ATLAS Collaboration, *Search for the Standard Model Higgs boson in the diphoton decay channel with 4.9 fb^{-1} of pp collision data at $\sqrt{s} = 7$ TeV with ATLAS*, Phys. Rev. Lett. **108** (2012) 111803.
[10] ATLAS Collaboration, *Search for the Standard Model Higgs boson in the decay channel $H \to ZZ^{(*)} \to 4\ell$ with 4.8 fb^{-1} of pp collision data at $\sqrt{s} = 7$ TeV with ATLAS*, Phys. Lett. **B 710** (2012) 383.
[11] ATLAS Collaboration, *Search for the Standard Model Higgs boson in the $H \to WW^{(*)} \to \ell\nu\ell\nu$ decay mode with 4.7 fb^{-1} of ATLAS data at $\sqrt{s} = 7$ TeV*, Physics Letters B **716** (2012) no. 1, 62 – 81, `arXiv:1206.0756 [hep-ex]`.
[12] ATLAS Collaboration, *Update of the $H \to WW^{(*)} \to e\nu\mu\nu$ analysis with 13.0 fb^{-1} of $\sqrt{s} = 8$ TeV data collected with the ATLAS detector*, 2012. `http://cdsweb.cern.ch/record/1493601`.
[13] LHC Higgs cross section working group, S. Dittmaier, C. Mariotti, G. Passarino, and R. Tanaka (Eds.), *Handbook of LHC Higgs Cross Sections: 2. Differential distributions*, 2012. `arXiv:1201.3084 [hep-ph]`. CERN-2011-002.
[14] ATLAS Collaboration, *The ATLAS experiment at the CERN large hadron collider*, JINST **3** (2008) S08003.